Langmuir

ARTICLE

pubs.acs.org/Langmuir

# Analysis of the Equilibrium Droplet Shape Based on an Ellipsoidal Droplet Model

Vlado A. Lubarda*[,†,‡] and Kurt A. Talke[†]

[†]Department of Mechanical and Aerospace Engineering, University of California—San Diego, La Jolla, California 92093-0411, United States

[‡]Montenegrin Academy of Sciences and Arts, Rista Stijovića 5, 81000 Podgorica, Montenegro

**ABSTRACT:** The extent of a droplet's spreading over a flat, smooth solid substrate and its equilibrium height in the presence of gravity are determined approximately, without a numerical solution of the governing nonlinear differential equation, by assuming that the droplet takes on the shape of an oblate spheroidal cap and by minimizing the corresponding free energy. The comparison with the full numerical evaluations confirms that the introduced approximation and the obtained results are accurate for contact angles below about 120° and for droplet sizes on the order of the capillary length of the liquid. The flattening effect of gravity is to increase the contact radius and decrease the height of the droplet, with these being more pronounced for higher values of the Bond number.

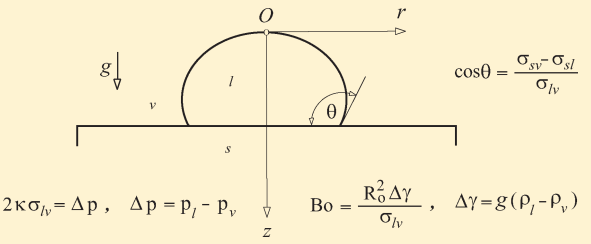


## 1. INTRODUCTION

The study of a droplet spreading over solid surfaces is a fundamental problem in the mechanics of wetting, which facilitates a better understanding of how to modify the properties of a surface to make it more or less wettable. This is of importance for various technological processes in the chemical and glass industry, in mechanical, electronic, soil, and rock engineering, in agriculture, and in biology.[1−3] For example, different methods of modifying the surface of polymerized material in order to make it more hydrophobic were recently investigated and quantitatively characterized by dynamic contact angle measurements, with an application to microfluidic chips.[4] In their study of microbead suspensions, often used in microfluidic devices for transporting biomolecules, Waghmare and Mitra[5] found that both the surface tension and the equilibrium contact angle decrease with an increase in the microbead volume fraction in the suspension. The equilibrium contact angle between a droplet and a substrate is also an important parameter in the study of water removal from the gas diffusion layer,[6] where a larger contact angle results in faster water removal. Recent experimental studies of electrowetting dynamics by Marinescu et al.[7] revealed that the contact angle hysteresis can be eliminated by applying short voltage pulses, in addition to the steady-state bias, because they facilitate the depinning of the contact line and activate the droplet motion. This is of importance for the analysis of systems that exploit the electrowetting effect, such as variable-focus lances, microfluidic systems, and electronic displays.

When a liquid droplet is slowly placed on a solid, flat substrate, it spreads to its equilibrium configuration with the macroscopic contact angle between the plane tangent to the droplet and a smooth substrate at the points of the three-phase (solid/liquid/vapor) intersection specified by Young's equation:[8]

$$\cos\theta = \frac{\sigma_{sv} - \sigma_{sl}}{\sigma_{lv}} \tag{1}$$

The surface energy (tension) between the two phases indicated by subscripts is denoted by $\sigma$. Thus, according to Young's equation, the contact angle $\theta$ is a material parameter dependent only on the involved surface energies. If the droplet spreads on a substrate in the absence of gravity, then the equilibrium shape is a spherical cap because for a given volume this shape minimizes the free energy of the system. The axisymmetric shape in the presence of gravity is more difficult to determine and requires the numerical integration of a nonlinear second-order differential equation

$$-\frac{r''}{(1 + r'^2)^{3/2}} + \frac{1}{r(1 + r'^2)^{1/2}} = \frac{2}{b} + \frac{\Delta\gamma}{\sigma_{lv}} z \tag{2}$$

The coordinate origin is taken at the top of the droplet, with the $z$ axis directed downward as shown in Figure 1. The superimposed prime denotes the derivative with respect to $z$. Equation 2 follows from Laplace's equation, relating the pressure difference across the surface of the droplet to its surface energy scaled by the mean curvature.[9,10] The liquid/vapor specific weight difference is $\Delta\gamma$. The radius of curvature at navel point O is denoted by $b$. The integration of eq 2 proceeds incrementally, starting from apex $z = 0$ of the droplet up to level $z = h$ at which the slope of the droplet matches Young's contact angle (eq 1), which is independent of gravity[11−13] The thus-determined value $z = h$ represents the actual height of the spread droplet and therefore the location of the substrate. Because $b$ is not known a priori, the integration procedure is iterative: the calculations are performed for various assumed values of $b$, and the true value of $b$ is determined a posteriori by matching it to the prescribed volume of the droplet.

**Received:** June 3, 2011
**Revised:** August 1, 2011
**Published:** August 03, 2011

The original calculations of this type were performed by Bashforth and Adams,[14] who provided extensive tables with the results corresponding to different values of nondimensional parameter $b^2\Delta\gamma/\sigma_{lv}$. More complete and accurate tables were later given by Padday.[15,16] These calculations, as well as the experimental observations, reveal that for droplets with a Young's contact angle below about 120° the equilibrium shape of the droplet is very nearly the shape of an axisymmetric ellipsoidal cap (i.e., an oblate spheroidal cap). Consequently, in this range of $\theta$, it is appealing to inquire if there is an alternative, simplified method to determine the equilibrium droplet configuration based on the energy minimization within the class of ellipsoidal droplet shapes without solving the nonlinear differential equation (eq 2). An ellipsoidal (oblate spheroid) droplet model was also adopted in an earlier study by Whyman and Bormashenko.[17]

The presented analysis in this article is restricted to a perfectly smooth surface of the substrate. A recent elaboration on the expression for the equilibrium contact angle of a droplet residing on a rough surface under different wetting conditions (Cassie–Baxter and Wenzel equations) can be found in refs 18 and 19. For example, if $r$ is the roughness factor of the surface of the substrate (the actual area divided by the projected area), then the Wenzel equation is obtained by replacing the numerator of Young's equation (eq 1) with $r(\sigma_{sv} - \sigma_{sl})$. Furthermore, in experiments it is often found that the three-phase contact line is immobile not only for $\theta = \theta_Y$ but also over the interval $\theta_r < \theta < \theta_a$. Angle $\theta_a$ is known as the advancing contact angle, and $\theta_r$ is known as the receding contact angle. The so-called contact angle hysteresis $\theta_a - \theta_r$ may be as much as 10° (or more), which is commonly attributed to the surface roughness, chemical contamination, or inhomogeneity.[20−22] For the study of the dynamics of the wetting process and the dynamic contact angle, see refs 20 and 23.

There are other ways in which gravity can affect the droplet's spreading and its equilibrium configuration, which are not discussed in this article. For example, Sakai and Fujii[24] found that the apparent contact angle on rough surfaces is raised by gravity, which they attributed to an increase in the interface energy between the solid and fluid phases caused by gravity because gravity works against gas adsorption (penetration) into the troughs of a rough surface (which by itself decreases the solid/liquid interface tension). The concept of a "fuzzy" solid/liquid interface was used by Letellier et al.[25] to describe substrates with ill-defined geometry (porous, structured, and fractal). Oscillations of liquid drops under gravity have been studied by Perez et al.[26] Other dynamic wetting problems are discussed in the review by Zisman[1] and in the book by de Gennes et al.[3] The effect of gravity on the shape of a pendant liquid droplet[10,16,27,28] or a liquid droplet placed vertically (on a vertical substrate) or on a tilted plane[29−32] has also been studied, but these studies are beyond the scope of this article.

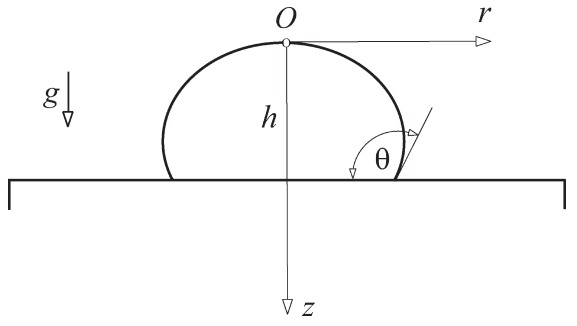


**Figure 1.** Equilibrium shape of a liquid droplet residing on a flat substrate in gravity field $g$. The equilibrium contact angle is $\theta$, and the height of the droplet is $h$. Coordinate origin O is at the apex of the droplet.

## 2. ELLIPSOIDAL DROPLET APPROXIMATION

Consider a liquid droplet of volume $V_0$ and specific weight $\gamma_l$ surrounded by its equilibrium vapor (or another less-dense liquid) with specific weight $\gamma_v$ as it is slowly deposited on a solid, flat substrate. Before touching the substrate, the droplet is assumed to be flattened in the vertical direction by gravity, as shown in Figure 2a, although the determination of this shape does not enter the subsequent analysis. Let $\sigma_{sv}$ be the surface energy (tension) of the solid/vapor interface, and let $\sigma_{lv}$ (henceforth denoted for simplicity by $\sigma$) be the surface energy of the liquid/vapor interface. The free energy of the system, which includes the surface of a flat substrate and the droplet in

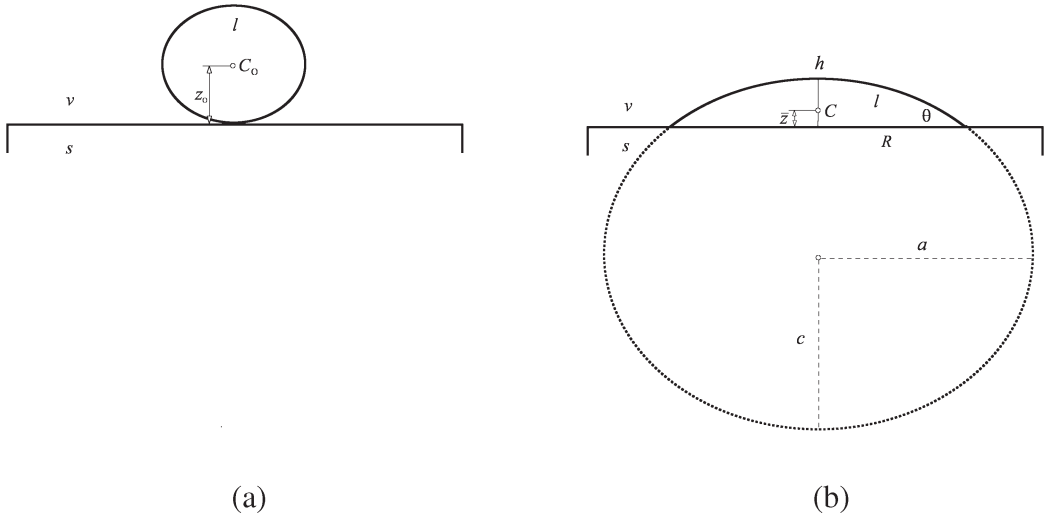


**Figure 2.** (a) Liquid droplet just before it is placed on top of a solid substrate. (b) Droplet configuration upon spreading into an ellipsoidal cap configuration. The contact angle is $\theta$, the radius of the circular solid/liquid interface is $R$, the height of the droplet is $h$, and its mass center is at a distance $\bar{z}$ above the surface of the substrate.

this initial configuration, is

$$E_0 = A_s\sigma_{sv} + S_0\sigma + V_0\bar{z}_0\Delta\gamma \quad (3)$$

where $A_s$ is the surface area of the substrate, $S_0$ and $V_0$ are the droplet's surface and volume, respectively, $\Delta\gamma = \gamma_l - \gamma_v$, and $\bar{z}_0$ is the elevation of the mass center $C_0$ of the droplet relative to the surface of the substrate. When the droplet is placed in contact with a flat, smooth solid substrate, depending on the physical and chemical properties of the involved substances, the droplet may wet the solid surface, spreading until it reaches its equilibrium configuration, such as shown in Figure 2b. The corresponding free energy of the system is

$$E = (A_s - \pi R^2)\sigma_{sv} + (\pi R^2)\sigma_{sl} + S\sigma + V\bar{z}\Delta\gamma \quad (4)$$

where $R$ is the radius of the circular region of the liquid/solid interface, $S$ and $V$ are the surface and the volume of the spreading droplet, and $\bar{z}$ is the elevation of the mass center $C$ of the droplet relative to the surface of the substrate. The solid/liquid interface energy is $\sigma_{sl}$. As discussed in the Introduction, the determination of the exact equilibrium shape of the droplet requires a numerical integration of the nonlinear differential equation (eq 2), keeping the volume of the droplet constant, and imposing appropriate boundary conditions at the top of the droplet and at contact points between the droplet and the substrate. Instead of this exact but semi-inverse procedure in which $b$ in eq 2 is not known a priori, we shall proceed by assuming that the equilibrium shape of the droplet is an axisymmetric ellipsoidal (oblate spheroidal) cap shape. This assumption, whose accuracy and range of validity will be evaluated a posteriori, significantly simplifies the analysis. The surface area of the spheroidal cap, whose cross section in the vertical plane of symmetry is shown in Figure 2b, can be readily obtained by integration,

$$S = \pi ac\left\{\frac{a}{c} - \left(1 - \frac{h}{c}\right)\left[1 + e^2\left(1 - \frac{h}{c}\right)^2\right]^{1/2} + \frac{1}{e}\left(\operatorname{arsinh}(e) - \operatorname{arsinh}\left[e\left(1 - \frac{h}{c}\right)\right]\right)\right\} \quad (5)$$

The unknown semiaxes of the ellipse are $a$ and $c$, and the height of the droplet is $h$. The eccentricity of the oblate spheroid is defined by

$$e^2 = \frac{a^2}{c^2} - 1 \geq 0 \quad (6)$$

and the function arsinh in eq 5 designates the inverse sine hyperbolic function. The volume of the ellipsoidal cap is

$$V = \frac{\pi}{3}a^2c\left(\frac{h}{c}\right)^2\left(3 - \frac{h}{c}\right) \quad (7)$$

Its centroid, relative to the surface of the substrate, is specified by

$$\bar{z} = \frac{h}{4}\frac{4 - \frac{h}{c}}{3 - \frac{h}{c}} \quad (8)$$

To proceed, it is convenient to introduce parametric equations of the ellipse in the vertical plane of symmetry so that at the contact point

$$\frac{R}{c} = \frac{a}{c}\sin\vartheta, \quad \frac{h}{c} = 1 - \cos\vartheta \quad (9)$$

By introducing eq 9 into eqs 5 and 7, we obtain

$$S = \frac{c}{a}\frac{\pi R^2}{\sin^2\vartheta}\left\{\frac{a}{c} - \cos\vartheta(1 + e^2\cos^2\vartheta)^{1/2} + \frac{1}{e}[\operatorname{arsinh}(e) - \operatorname{arsinh}(e\cos\vartheta)]\right\} \quad (10)$$

$$V = \frac{\pi}{3}\frac{c}{a}\frac{R^3}{\sin^3\vartheta}(1 - \cos\vartheta)^2(2 + \cos\vartheta) \quad (11)$$

Furthermore, from eq 8, we have

$$\bar{z} = \frac{c}{a}\frac{R}{\sin\vartheta}\frac{(1 - \cos\vartheta)(3 + \cos\vartheta)}{4(2 + \cos\vartheta)} \quad (12)$$

If the liquid of a droplet is incompressible and if there is no evaporation during its spreading, the constant volume condition $V = V_0$ gives

$$\frac{R}{R_0} = \frac{2^{2/3}\sin\vartheta}{(c/a)^{1/3}(1 - \cos\vartheta)^{2/3}(2 + \cos\vartheta)^{1/3}}$$
$$\frac{c}{R_0} = \frac{2^{2/3}(c/a)^{2/3}}{(1 - \cos\vartheta)^{2/3}(2 + \cos\vartheta)^{1/3}} \quad (13)$$

where $R_0$ is the radius of an imagined spherical droplet with volume $V_0 = (4\pi/3)R_0^3$.

## 3. FREE-ENERGY MINIMIZATION

Within the class of the considered ellipsoidal cap shapes, the equilibrium droplet configuration minimizes the free energy $E$ in eq 4. This energy depends on the parameter $\vartheta$ and the aspect ratio $c/a$ (i.e., $E = E(\vartheta, c/a)$), and thus the necessary minimization conditions are $\partial E/\partial\vartheta = 0$ and $\partial E/\partial(c/a) = 0$. These conditions give two simultaneous nonlinear equations for $\vartheta$ and $c/a$, which must be solved numerically. The location of the energy minimum of the function $E = E(\vartheta, c/a)$ can be found numerically, without deriving the explicit form of the stationary conditions. For such calculations, the free-energy expression (scaled by $R_0^2\pi\sigma$) is written as

$$\frac{E}{R_0^2\pi\sigma} = -(\cos\theta_Y)f_1(\vartheta, c/a) + f_2(\vartheta, c/a) + Bof_3(\vartheta, c/a) \quad (14)$$

where the auxiliary nondimensional functions are defined by

$$f_1 = \frac{2^{4/3}(1 + \cos\vartheta)}{(c/a)^{2/3}(1 - \cos\vartheta)^{1/3}(2 + \cos\vartheta)^{2/3}}$$
$$f_3 = \frac{2^{2/3}(1 - \cos\vartheta)^{1/3}(3 + \cos\vartheta)}{3(a/c)^{2/3}(2 + \cos\vartheta)^{4/3}} \quad (15)$$

$$f_2 = \frac{c}{a}\frac{f_1}{\sin^2\vartheta}\left\{\frac{a}{c} - \cos\vartheta(1 + e^2\cos^2\vartheta)^{1/2} + \frac{1}{e}[\operatorname{arsinh}(e) - \operatorname{arsinh}(e\cos\vartheta)]\right\} \quad (16)$$


dx.doi.org/10.1021/la202077w |Langmuir 2011, 27, 10705–10713

**Table 1. Surface Tension $\sigma$, Specific Weight $\gamma$, and Capillary Length $l = (\sigma/\gamma)^{1/2}$ for Selected Liquids in Contact with Air at Room Temperature**

| liquid | $\sigma$ (N/m) | $\gamma$ (kN/m$^3$) | $l$ (mm) |
|---|---|---|---|
| benzene | 0.029 | 8.6 | 1.84 |
| blood | 0.058 | 10.4 | 2.36 |
| carbon tetrachloride | 0.0264 | 15.59 | 1.3 |
| ethanol | 0.0224 | 7.75 | 1.7 |
| ethylene glycol | 0.0473 | 11.04 | 2.07 |
| Fromblin Zdol | 0.022 | 20 | 1.05 |
| glycerin | 0.063 | 12.4 | 2.25 |
| mercury | 0.486 | 133.7 | 1.9 |
| water | 0.073 | 9.81 | 2.73 |

The surface-energy parameter is

$$\cos\theta_Y = \frac{\sigma_{sv} - \sigma_{sl}}{\sigma} \tag{17}$$

The nondimensional number

$$Bo = \frac{R_0^2 \Delta\gamma}{\sigma} \tag{18}$$

represents the effect of gravity relative to the surface tension, referred to in the fluid mechanics literature as the Bond number. The latter can also be expressed as $Bo = (R_0/l)^2$, where the length scale $l = (\sigma/\Delta\gamma)^{1/2}$ is known as the capillary length.[2] Clearly, $Bo$ is less than 1% if $R_0$ is less than 1/10 of $l$. For a water droplet in air, $\Delta\gamma = 9.8$ kN/m$^3$ and $\sigma = 0.073$ N/m so that the capillary length $l = 2.73$ mm. Brunner et al.[33] deposited droplets of a perfluoropolyether-type lubricant, known as Fomblin Zdol, on a solid, smooth surface coated with a layer of nitrogenated carbon ($CN_x$), typically used in hard disk drives. They considered surface energies in the range of $\sigma = (16 - 25.5) \times 10^{-3}$ J/m$^2$ and $\sigma_{sv} = 52.3 \times 10^{-3}$ J/m$^2$. In this case, with $\Delta\gamma = 20$ kN/m$^3$ and $\sigma = 0.022$ J/m$^2$, the capillary length is $l = 1.05$ mm. Thus, gravity imposes a more appreciable effect on Fromblin Zdol than on water droplets. Table 1 lists the capillary length for selected liquids in contact with air at room temperature.

It should also be pointed out that the accurate analytical and experimental estimates of $\sigma_{sv}$ and $\sigma_{sl}$ are still challenging. For example, surface energy $\sigma_{sl}$ depends on solid and liquid bonding and the attractive van der Waals interactions between the solid and liquid near their interface. Experimental methods of measuring surface tension by using sessile and pendant drops and bubbles, as well as other means, have recently been discussed in ref 10.

Upon finding minimizers $\vartheta$ and $c/a$ of the energy expression (eq 14), the extent of a droplet's spreading ($R$) and its height ($h$) are determined numerically from eqs 9 and 13. The corresponding value of the equilibrium contact angle is $\theta = \arctan[(c/a)\tan\vartheta)]$ because the slope at the contact point is $\tan\theta = ((c/a)^2R)/(c - h)$, and in view of eq 9, $(c/a) = (\tan\theta)/(\tan\vartheta)$. As discussed in sections 4 and 5 for droplet sizes on the order of the capillary length of the liquid and for $\theta_Y$ in eq 17 that is less than about 120°, the predicted value of the contact angle ($\theta$) is only slightly different from the Young's value of the contact angle ($\theta_Y$) because in these cases the ellipsoidal shape of the droplet is an excellent approximation of the droplet's shape obtained by solving the nonlinear differential equation (eq 2).

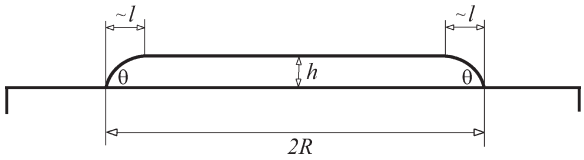


**Figure 3.** Paddle of a nearly constant thickness $h$ and radius $R$. The extent of the edge effects near the contact line is on the order of the capillary length, $l$. The wetting contact angle is $\theta$.

Next we consider limiting cases $Bo \ll 1$ and $Bo \gg 1$. If $Bo \ll 1$, then the last (gravity) term on the right-hand side of eq 14 can be neglected and the energy analysis leads the spherical cap shape of a droplet ($a = c$, $e = 0$, $\vartheta = \theta$). In this case, $f_2 = 2f_1/(1 + \cos\theta)$ and the stationary condition $\partial E/\partial\theta = 0$ yields $\cos\theta = \cos\theta_Y$ (i.e., the equilibrium contact angle is given by Young's equation (eq 1)). For the completeness of the analysis, an independent analysis of the equilibrium droplet's shape in the absence of gravity is presented in the Appendix. The perturbation methods and the matched asymptotic expansions, with the Bond number as a small parameter, were also used to study the shape of small and large sessile drops.[34] The matched asymptotic expansions were earlier used in ref 35 to examine the validity of Young's expression for small values of the ratio of the range of intermolecular forces and a typical macroscopic length of the problem. See also ref 36 for an analytical study of the shape of a liquid−vapor interface within and outside the molecular region, with particular reference to the determination of the point on the vapor−liquid interface, within a thin transition region, where the angle of inclination is equal to the macroscopic contact angle.

If $Bo \gg 1$, then the gravity effects are so dominant that a drop takes on the shape of a paddle whose thickness $h$ is nearly constant everywhere, except near the edges of a paddle (Figure 3). Because the extent of the edge effects is expected to be on the order of the capillary length $l \ll R$,[3] the free energy of the system is approximately and up to a constant term

$$\begin{aligned} E &= \pi R^2(\sigma + \sigma_{sl} - \sigma_{sv}) + V_0(h/2)\Delta\gamma \\ R^2\pi h &\approx V_0 = (4/3)R_0^3\pi \end{aligned} \tag{19}$$

The stationary condition $\partial E/\partial h = 0$ then gives

$$\begin{aligned} \frac{h}{R_0} &= 2(Bo)^{-1/2}\sin(\theta_Y/2) \\ \frac{R}{R_0} &= \left[\frac{2(Bo)^{1/2}}{3\sin(\theta_Y/2)}\right]^{1/2} \end{aligned} \tag{20}$$

The expression for $h$ in eq 20 can be rewritten as $h = 2l\sin(\theta_Y/2)$, in agreement with eq 2.10 in de Gennes et al.[3]

## 4. NUMERICAL EVALUATION OF THE GRAVITY EFFECT

Figure 4 shows the equilibrium values of $\cos\theta$, corresponding to the prescribed values of $\cos\theta_Y = (\sigma_{sv} - \sigma_{sl})/\sigma \in [-1, 1]$ and the selected values of the Bond number $Bo$. In both figures, the solid line corresponds to Young's equation ($Bo = 0$). As seen in Figure 4a, for $Bo < 0.5$ the agreement between the predicted contact angle and Young's value is excellent, except for hydrophobic surfaces with $\theta_Y$ greater than about 120°. In these cases, the ellipsoidal approximation of a droplet's shape is expected to be sufficiently accurate, as confirmed in section 5. Figure 5a shows the corresponding variation of the (normalized) extent of

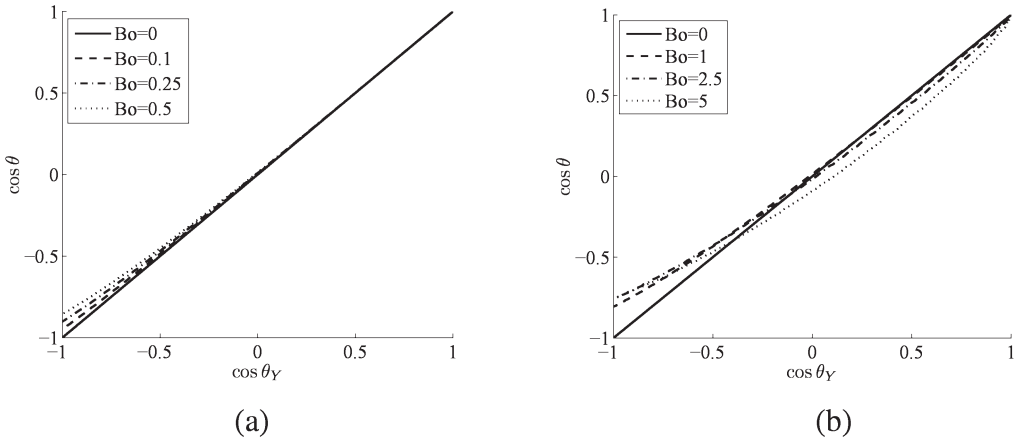


**Figure 4.** (a) Variation of the equilibrium value of cos $\theta$ with cos $\theta_Y = (\sigma_{sv} - \sigma_{sl})/\sigma$ for an ellipsoidal droplet model and the indicated values of the Bond number. (b) The same in the case of 10 times higher values of the Bond number.

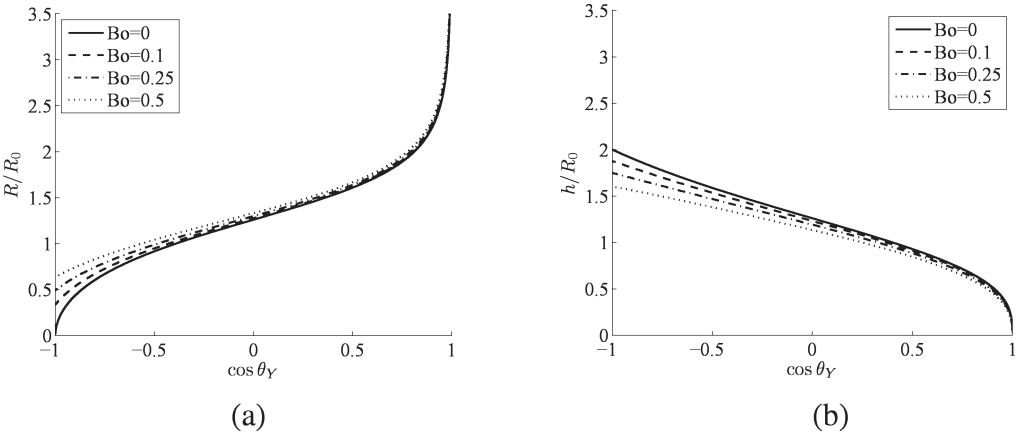


**Figure 5.** (a) Variation of the extent of equilibrium spreading $(R/R_0)$ with cos $\theta_Y = (\sigma_{sv} - \sigma_{sl})/\sigma$ for an ellipsoidal droplet model. (b) Corresponding variation of the normalized height of the droplet $(h/R_0)$. The normalizing radius is $R_0 = (3V_0/4\pi)^{1/3}$, where $V_0$ is the volume of the droplet.

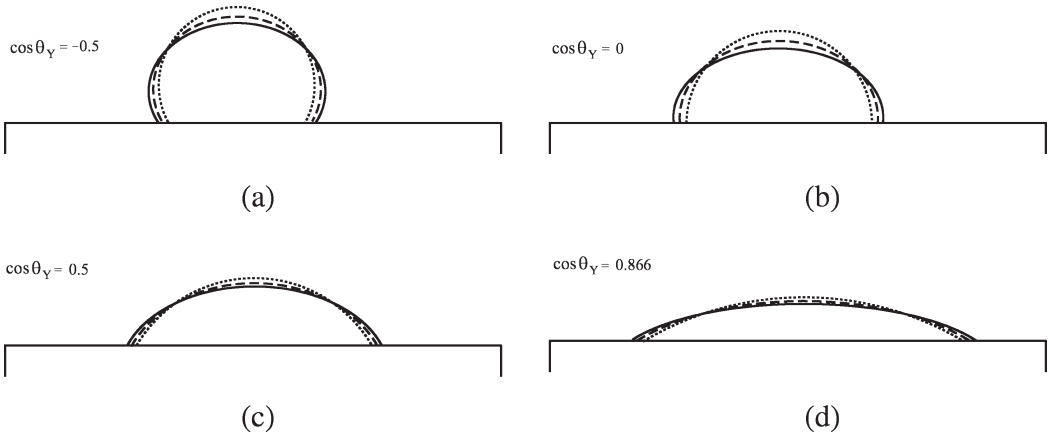


**Figure 6.** Cross section of the spread droplet in the plane of its symmetry in the case of $Bo = 0$ (···), 0.5 (---), and 1 (—). The four cases correspond to four different values of surface-energy parameter cos $\theta_Y$, as indicated.

spreading $(R/R_0)$, and Figure 5b shows the variation of the (normalized) height of the droplet $(h/R_0)$. Figure 6 shows the cross section of the spread droplet in the plane of its symmetry corresponding to $Bo = 0$, 0.5, and 1. The four cases correspond to four different values of surface-energy parameter cos $\theta_Y$ ($3^{1/2}/2$, 0.5, 0, and −0.5). In each case, the flattening effect of gravity is to increase the contact radius $R$ and decrease the height of the droplet $h$, with these being more pronounced for higher values of the Bond number. The departure from the spherical cap shape also increases with $Bo$. For example, in the case of $Bo =$


dx.doi.org/10.1021/la202077w |*Langmuir* 2011, 27, 10705–10713

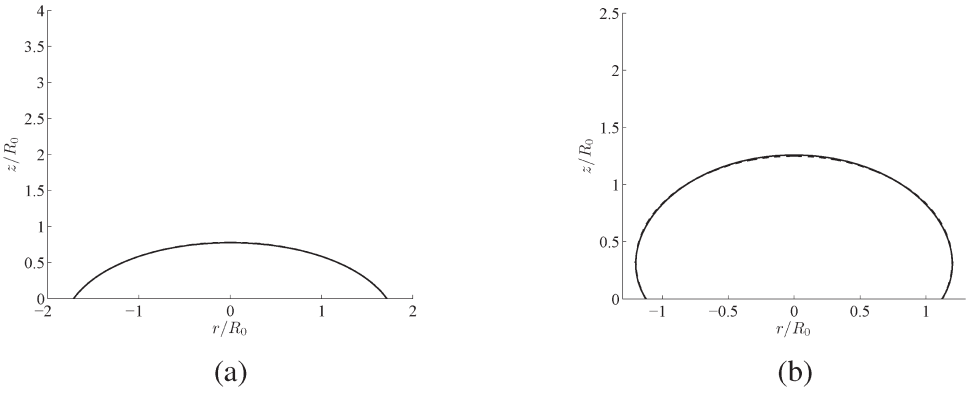


**Figure 7.** Solid line showing the droplet profile obtained by the numerical integration of eq 21. The dashed line (barely seen) is obtained from the ellipsoidal droplet model. The Young's contact angles are (a) $\theta = 60°$ and (b) $\theta = 120°$. In both cases, the Bond number is $Bo = 1$.

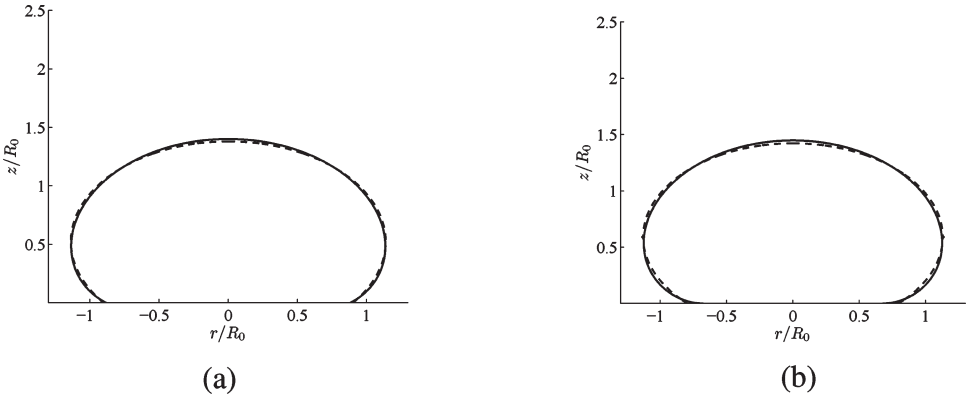


**Figure 8.** Solid line showing the droplet profile obtained by the numerical integration of eq 21. The dashed line is obtained from the ellipsoidal droplet model. The Young's contact angles are (a) $\theta = 150°$ and (b) $\theta = 180°$. In both cases, the Bond number is $Bo = 1$.

0.25, the semiaxes ratio of the ellipsoidal (oblate spheroid) shape is $c/a = 0.653$, but in the case of $Bo = 1$, this ratio is $c/a = 0.354$, which is far below the value of 1 corresponding to a spherical cap shape.

For $Bo > 1$, the ellipsoidal shape approximation is less satisfactory, particularly for higher values of $Bo$ (Figure 4b). For very large values of the Bond number ($Bo \gg 1$), the equilibrium shape of a liquid is that of a nearly flat paddle (Figure 3), as discussed in section 3.

## 5. COMPARISON WITH THE RESULTS FROM THE NUMERICAL INTEGRATION OF ODE

The results from section 4, based on the ellipsoidal droplet model, are now compared with the calculations obtained by the numerical integration of differential eq 2. The integration proceeds iteratively: the unknown radius of curvature $b$ is assumed, and eq 2 is integrated until the slope $r'(h)$ matches Young's angle $\theta_Y$, calculated from eq 17 (i.e., $r'(h) = \cot \theta_Y$). The boundary conditions at the origin are $r(0) = 0$ with an infinite slope $r'(0)$. The obtained solution applies to a droplet with the volume corresponding to thus-calculated $r = r(z)$ and $h$. The nondimensional version of eq 2 is

$$-\frac{\bar{r}''}{(1 + \bar{r}'^2)^{3/2}} + \frac{1}{\bar{r}(1 + \bar{r}'^2)^{1/2}} = 2 + (b/R_0)^2 Bo\bar{z} \quad (21)$$

where $\bar{r} = r/b$ and $\bar{z} = z/b$.

Figure 7 shows excellent agreement between the predicted shapes of liquid droplets obtained by the ellipsoidal droplet model and by the described numerical solution of eq 21. In Figure 7a, the Young's contact angle is $\theta_Y = 60°$, and in Figure 7b, it is $\theta_Y = 120°$. The results correspond to the Bond number $Bo = 1$ so that $R_0 = l$. In Figure 7a, the semiaxes of the ellipsoidal model are $a = 1.83R_0$ and $c = 1.195R_0$. The extent of spreading is $R = 1.716R_0$, and the height of the droplet is $h = 0.78R_0$. The predicted contact angle is $\theta = 60.4°$. The radius of curvature at the apex point of the droplet is $a^2/c = 2.8R_0$. The radius of curvature obtained by the integration of eq 21, for the same droplet volume $V = (4\pi/3)R_0^3$ is $b = 2.9R_0$. The corresponding extent of spreading is $R = 1.7156R_0$, and the height of the droplet is $h = 0.776R_0$.

In Figure 7b, the semiaxes of the ellipsoidal model are $a = 1.199R_0$ and $c = 0.928R_0$. The extent of spreading is $R = 1.1238R_0$, and the height of the droplet is $h = 1.25R_0$. The predicted contact angle is $\theta = 115.6°$. The radius of curvature at the apex point of the droplet is $1.549R_0$. The radius of curvature for the same droplet volume and a contact angle of $\theta = 120°$ is $b = 1.487R_0$. The corresponding extent of spreading is $R = 1.1214R_0$, and the height of the droplet is $h = 1.259R_0$.

Figure 8 shows the droplet shapes when the Young's contact angle is $\theta_Y = 150$ and $180°$ and the Bond number is $Bo = 1$. In Figure 8a, the semiaxes of the ellipsoidal model are $a = 1.138R_0$ and $c = 0.856R_0$. The extent of spreading is $R = 0.9R_0$, and the height of the droplet is $h = 1.38R_0$. The predicted contact angle is

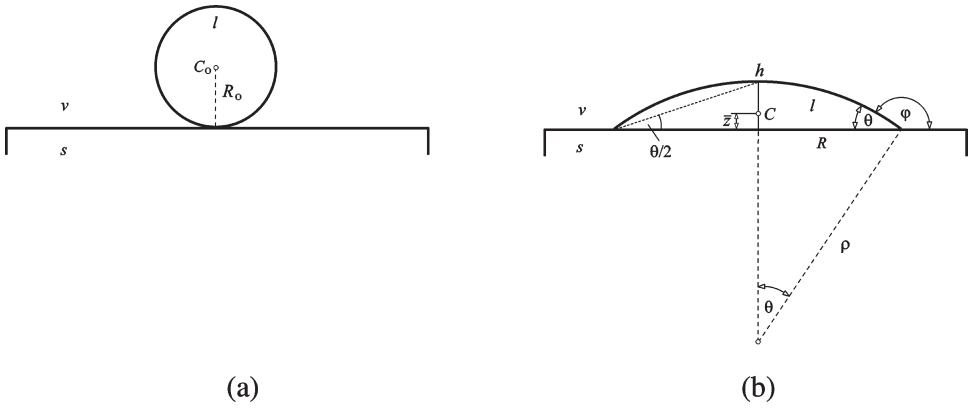


**Figure 9.** (a) Spherical droplet of radius $R_0$ just before touching the solid substrate. (b) Droplet configuration upon spreading into the spherical cap configuration. The contact angle is $\theta$, the radius of the solid/liquid interface is $R$, the height of the droplet is $h$, and the radius of the curvature of the liquid/vapor interface is $\rho$.

$\theta$ = 135.8°. The radius of curvature at the apex point of the droplet is $1.513R_0$. The radius of curvature obtained by the integration of eq 21 for the same droplet volume is $b = 1.379R_0$. The corresponding extent of spreading is $R = 0.88R_0$, and the height of the droplet is $h = 1.4R_0$.

In Figure 8b, the semiaxes of the ellipsoidal model are $a = 1.129R_0$ and $c = 0.831R_0$. The extent of spreading is $R = 0.795R_0$, and the height of the droplet is $h = 1.4213R_0$. The predicted contact angle is $\theta$ = 144°, which is substantially lower than what the actual contact angle should be (180°). The radius of curvature at the apex point of the droplet is $1.534R_0$. The radius of curvature for the same droplet volume is $b = 1.36R_0$. The corresponding extent of spreading is $R = 0.676R_0$, and the height of the droplet is $h = 1.4472R_0$.

An experimental determination of the shape of sessile droplets has been conducted by Ren et al.,[30] Padday and Pitt,[37] Li et al.,[38] and Naydich et al.,[39] among others. The results from these investigations support the ellipsoidal approximation in the considered range of the droplet's size and the equilibrium contact angle. (See, for example, Figure 5 in ref 38.) A quantitative comparison of our theoretical results with available experimental data depends on the involved solid/liquid system and the smoothness of the substrate surface because the surface roughness, chemical contamination, and inhomogeneities give rise to contact angle hysteresis, which may be 10° or more.[20] A more specific comparison with experimental data may require an extension of the analysis to incorporate some of these effects as well as more reliable data on the solid/liquid interface energy for different systems, which is left for future investigations.

## 6. CONCLUSIONS

The equilibrium spreading of a liquid droplet over a flat, smooth solid substrate in the presence of gravity has been studied by assuming that the droplet takes on an ellipsoidal shape. The extent of a droplet's spreading and its equilibrium height are determined approximately, without numerical solution of the governing nonlinear differential equation, by applying the free-energy minimization within the class of the oblate spheroidal shapes. The comparison with the full numerical evaluations reveals that the obtained results are accurate for contact angles below 120° and for droplet sizes on the order of the capillary length of the liquid ($Bo < 1$). The flattening effect of gravity is to increase the contact radius and decrease the height of the droplet. For larger values of the Bond number ($Bo > 1$), the ellipsoidal approximation of a droplet's shape is less satisfactory, particularly for higher values of the Young's contact angle. For $Bo \gg 1$, the liquid takes on the shape of a nearly flat paddle, except near its edges. The ellipsoidal approximation may also be important for the dynamic study of a droplet's spreading by means of the mechanics of configurational forces, which otherwise requires an involved solution of partial differential equations from fluid mechanics.[40,41]

## APPENDIX: SPHERICAL AND CYLINDRICAL DROPLET MODELS

For the completeness of the analysis, we summarize the results for spherical and cylindrical droplets in the absence of gravity.[19,42,43] The initial free energy of the system in Figure 9a is $E_0 = A_s\sigma_{sv} + S_0\sigma$, where $S_0 = 4\pi R_0^2$ is the droplet's surface area and $A_s$ is the area of the flat surface of the solid substrate. When the droplet spreads over the flat, smooth substrate, the free energy of the configuration shown in Figure 9b is

$$E = (A_s - \pi R^2)\sigma_{sv} + (\pi R^2)\sigma_{sl} + S\sigma + (2\pi R)\tau \qquad (22)$$

where $R$ is the radius of the circular region of the liquid/solid interface and $S$ and $V$ are the top surface and the volume of the spread droplet. For generality, we also include in eq 22 the line tension $\tau$ (per unit length) associated with the excess free energy due to atomic or molecular rearrangements around the triple-phase contact line. By using geometric relations for spherical cap geometry,[44] we have

$$S = 2\pi\rho h,\ V = \frac{\pi}{6}h(3R^2 + h^2) \qquad (23)$$

The height of the spread droplet is $h = R\tan(\theta/2)$, which can be used to determine the slope $\theta$ by measuring $R$ and $h$ as $\theta = 2\arctan(h/R)$. The radius of curvature of the surface of the droplet is $\rho = R/\sin\theta$. Equation 23 can be written in terms of $R$ and $\theta$ as

$$S = 2\pi R^2\frac{1}{1+\cos\theta},\ V = \frac{1}{3}\pi R^3\frac{(2+\cos\theta)\sin\theta}{(1+\cos\theta)^2} \qquad (24)$$

Some liquid evaporation is inevitable, unless the atmosphere surrounding the droplet is saturated with the vapor of the liquid. The effect of evaporation on the contact angle between the droplet and the substrate has been studied extensively (e.g., refs 45 and 46.) However, if it is assumed that there is no evaporation during droplet spreading and that the liquid of the droplet

is incompressible, then constant-volume conditions $V = V_0 = (4\pi/3)R_0^3$ and $dV/d\theta = 0$ give

$$R = \frac{2^{2/3}R_0 \sin\theta}{(1-\cos\theta)^{2/3}(2+\cos\theta)^{1/3}} \qquad R\frac{d\theta}{dR} = -(2+\cos\theta)\sin\theta \tag{25}$$

The energy dissipated by viscous flow during the spreading of the droplet and by the friction between the expanding contact line of the droplet and the solid substrate is $\phi = E_0 - E$. The function $\phi = \phi(\varphi)$ is a monotonically increasing function of the angle $\varphi = \pi - \theta$, with $\phi(0) = 0$ (dissipation increases with spreading). Correspondingly, $E = E(\varphi)$ is a monotonically decreasing function of $\varphi$, with $E(0) = E_0$. The droplet spreading begins at $\varphi = 0$ and ceases at $\varphi = \varphi_{eq}$, which minimizes $E(\varphi)$ and maximizes $\phi(\varphi)$ because the dissipated energy increases as $\varphi$ increases from the initial angle $\varphi = 0$ to the equilibrium angle $\varphi = \varphi_{eq}$. If $E$ takes the minimum value at the boundary of the interval $[0, \pi]$, then the droplet does not spread at all ($\varphi_{eq} = 0$) or it spreads completely into an infinitesimally thin film ($\varphi_{eq} = \pi$). If $0 < \varphi_{eq} < \pi$, then the function $E = E(\varphi)$ has its minimum within the interval $[0, \pi]$, corresponding to the stable equilibrium configuration of the droplet. Consequently, its equilibrium configuration is determined by the stationary condition $\partial E/\partial\theta = 0$.[19,42,43]

**A.1. Configurational Force.** An alternative derivation of the equilibrium condition is based on the concept of the configurational force. A comprehensive treatment of configurational forces in a wide variety of mechanics problems can be found in the monograph by Gurtin[47] and the reviews by Maugin[48] and Suo.[49] The configurational force ($F$) on the droplet (per unit length of its three-phase contact line) is orthogonal to the contact line and is defined such that

$$(2\pi R)F = -\frac{\partial E}{\partial R} \tag{26}$$

By differenting eq 22 with respect to $R$, we have

$$\frac{\partial E}{\partial R} = -2\pi R(\sigma_{sv} - \sigma_{sl}) + \frac{\partial S}{\partial R}\sigma + 2\pi\tau \tag{27}$$

In view of eq 25, from eq 24 there follows $\partial S/\partial R = 2\pi R\cos\theta$, and substitution into eqs 26 and 27 yields

$$F = \sigma\left(\frac{\sigma_{sv} - \sigma_{sl}}{\sigma} - \cos\theta - \frac{\tau}{R\sigma}\right) \tag{28}$$

The droplet reaches its equilibrium configuration when the configurational force vanishes, which gives a transcendental equation for the equilibrium contact angle,

$$\cos\theta + \frac{\tau}{R(\theta)\sigma} = \frac{\sigma_{sv} - \sigma_{sl}}{\sigma} \tag{29}$$

If the line tension is ignored, then eq 29 reduces to Young's equation (eq 1) for the (macroscopic) equilibrium contact angle. Thus, the equilibrium contact angle depends on $\sigma$ and the surface-energy difference $\sigma_{sv} - \sigma_{sl}$ but is independent of the size of the droplet. Hard solids (with covalent, ionic, or metallic bonding) have high surface energies (0.5−5 J/m$^2$), but weak solids (bonded by van der Waals forces) have low surface energies (~0.05 J/m$^2$).[20] In a microscopically small region near the three-phase contact line, the shape of the droplet profile may have a rapid variation of its tangent angle,[50] which cannot be predicted by macroscopic analysis.

If the line tension effect is retained so that the spreading of the droplet is driven by the conversion of the surface and line energies, then the contact angle is governed by eq 29, which is known as the generalized or modified Young's equation (sometimes also referred to as the Boruvka−Neumann equation[51] after the generalization of the classical theory of capillary by Boruvka and Neumann;[52] see also ref 53). In this case, the equilibrium contact angle depends not only on the three interfacial surface energies ($\sigma$, $\sigma_{sv}$, and $\sigma_{sl}$) but also on the line tension and the size of the initial droplet. If $\tau$ is positive, then $\theta$ is larger for larger $\tau$ and vice versa (i.e., the wetting is more pronounced in systems with smaller line tensions). As discussed by Widom,[54] this can be visualized as the effect of tightening or loosening the "collar" (the three-phase contact line).

**A.2. Cylindrical Droplet.** The analysis of the equilibrium contact angle for a cylindrical droplet, which is infinitely long in the direction orthogonal to the plane of the drawing shown in Figure 9, is of importance because there have been many numerical calculations of the droplet's spreading based on molecular interactions using a 2D cylindrical droplet model in order to reduce the extensive computational time.[55,56] There has also been an analytical study of the shape of a 2D droplet in equilibrium with a surrounding thin film on a solid substrate in which a disjoining−conjoining pressure accounts for intermolecular forces between the solid and the liquid.[57] The apparent contact angle, defined in this study as the angle between the surface and the substrate at the inflection point in the contact line region, is shown to depend on the size (cross-sectional area) of a 2D droplet in such a way that the cylindrical cap is a good approximation only for large droplets.

The configurational force for driving the spreading of the cylindrical droplet (per unit length), one on each of the two ends of the droplet, is defined by

$$F = -\frac{1}{2}\frac{\partial E}{\partial R} \tag{30}$$

where $E$ is the free energy of the system per unit length. Ignoring gravity and thus assuming circular geometry, the free energy is

$$E = (L_s - 2R)\sigma_{sv} + 2R\sigma_{sl} + \frac{2R\theta}{\sin\theta}\sigma + 2\tau \tag{31}$$

The length of the top edge of the substrate before wetting is $L_s$, the in-plane spread of the solid/liquid interface is $2R$, and $2R\theta/\sin\theta$ is the length of the upper circular edge of the droplet (liquid/vapor interface). The incompressibility constraint for the cylindrical droplet implies that during its spreading the cross-sectional area of the droplet is constant and equal to $R_0^2\pi$:

$$R^2\frac{\theta - \sin\theta\cos\theta}{\sin^2\theta} = R_0^2\pi \tag{32}$$

Consequently,

$$R = R_0\frac{\pi^{1/2}\sin\theta}{(\theta - \sin\theta\cos\theta)^{1/2}} \qquad R\frac{d\theta}{dR} = \frac{\sin\theta(\theta - \sin\theta\cos\theta)}{\theta\cos\theta - \sin\theta} \tag{33}$$

and from eqs 30 and 31 we obtain

$$F = \sigma_{sv} - \sigma_{sl} - \sigma \cos\theta \quad (34)$$

The configurational force on a cylindrical droplet does not depend on $\tau$ because the line tension contribution to the free energy is constant and equal to $2\tau$ throughout the spreading of the droplet. In the equilibrium configuration of the droplet, the configurational force in eq 34 vanishes, which gives Young's eq 1.

## AUTHOR INFORMATION


### Corresponding Author

*Tel: 858-534-3169. Fax: 858-534-5698. E-mail: vlubarda@ucsd.edu.


## ACKNOWLEDGMENT

Research support from the Montenegrin Academy of Sciences and Arts and the MAE endowment fund at UCSD are acknowledged. We also thank Professor Frank E. Talke for valuable discussions on the mechanics of wetting phenomena and the reviewers for their helpful comments and suggestions.

## REFERENCES


(1) Zisman, W. In *Contact Angle, Wettability, and Adhesion*; Gould, R. F., Ed.; Advances in Chemistry Series; American Chemical Society: Washington, DC, 1964; p 43, Chapter 1.

(2) Rowlinson, J. S.; Widom, B. *Molecular Theory of Capillarity*; Clarendon: Oxford, U.K., 1982.

(3) de Gennes, P. G.; Brochard-Wyart, F.; Quéré, D. *Capillarity and Wetting Phenomena*; Springer: Berlin, 2004.

(4) Wägli, Ph.; Homsy, A.; de Rooij, N. F. *Sens. Actuators, B* **2011**, *156*, 994–1001.

(5) Waghmare, P. R.; Mitra, S. K. *Langmuir* **2010**, *26*, 17082–17089.

(6) Park, J. W.; Jiao, K.; Li, X. *Appl. Energy* **2010**, *87*, 2180–2186.

(7) Marinescu, M.; Urbakh, M.; Barnea, T.; Kucernak, A. R.; Kornyshev, A. A. *J. Phys. Chem. C* **2010**, *114*, 22558–22565.

(8) Young, T. *Philos. Trans. R. Soc. London* **1805**, *95*, 65–87.

(9) Batchelor, G. K. *An Introduction to Fluid Dynamics*; Cambridge University Press: Cambridge, U.K., 1967.

(10) Miller, C. A.; Neogi, P. *Interfacial Phenomena: Equilibrium and Dynamic Effects*, 2nd ed.; CRC Press: Boca Raton, FL, 2008; pp 1−59.

(11) Johnson, R. E. *J. Phys. Chem.* **1959**, *63*, 1655–1658.

(12) Blokhuis, E. M.; Shilkrot, Y.; Widom, B. *Mol. Phys.* **1995**, *86* 891–899.

(13) Larher, Y. *Langmuir* **1997**, *13*, 7299–7300.

(14) Bashforth, F.; Adams, J. C. *An Attempt to Test the Theory of Capillary Action*; Cambridge University Press: Cambridge, U.K., 1893.

(15) Padday, J. F. *Surface and Colloid Science*; Matijevic, E., Ed.; Wiley: New York, 1969; pp 101−151.

(16) Padday, J. F. In *Capillarity Today*; Pétré, G., Sanfeld, A., Eds.; Lecture Notes in Physics; 386; Springer: New York,1991; pp 90−107.

(17) Whyman, G.; Bormashenko, E. *J. Coll. Interface Sci.* **2009**, *331*, 174–177.

(18) He, B.; Patankar, N. A.; Lee, J. *Langmuir* **2003**, *19*, 4999–5003.

(19) Whyman, G.; Bormashenko, E.; Stein, T. *Chem. Phys. Lett.* **2008**, *450*, 355–359.

(20) de Gennes, P. G. *Rev. Mod. Phys.* **1985**, *57*, 827–863.

(21) Tadmor, R.; Yadov, P. S. *J. Colloid Interface Sci.* **2008**, *317*, 241–246.

(22) Tadmor, R. *Soft Matter* **2011**, *7*, 1577–1580.

(23) de Ruijter, M. J.; Blake, T. D.; De Coninck, J. *Langmuir* **1999**, *15*, 7836–7847.

(24) Sakai, H.; Fujii, T. *J. Colloid Interface Sci.* **1999**, *210*, 152–156.

(25) Letellier, P.; Mayaffre, A.; Turmine, M. *J. Colloid Interface Sci.* **2007**, *314*, 604–614.

(26) Perez, M.; Brechet, Y.; Salvo, L.; Papoular, M.; Suery, M. *Europhys. Lett.* **1999**, *47*, 189–195.

(27) del Río, O. I.; Neumann, A. W. *J. Colloid Interface Sci.* **1997**, *196* 136–147.

(28) Tadmor, R.; Bahadur, P.; Leh, A.; N'guessan, H. E.; Jaini, R.; Dang, L. *Phys. Rev. Lett.* **2009**, *103*, 266101.

(29) Finn, R. *Not. AMS* **1999**, *46*, 770–781.

(30) Ren, H.; Xu, S.; Wu, S.-T. *Opt. Commun.* **2010**, *283*, 3255–3258.

(31) Quére, D.; Marie-José Azzopardi, M.-J.; Delattre, L. *Langmuir* **1998**, *14*, 2213–2216.

(32) Pu, G.; Ai, J.; Severtson, S. J. *Langmuir* **2010**, *26*, 12696–12702.

(33) Brunner, R.; Etsion, I.; Talke, F. E. *Langmuir* **2009**, *26*, 1824–1829.

(34) Homentcovschi, D. *Acta Mech.* **1998**, *128*, 141–171.

(35) Merchant, G. J.; Keller, J. B. *Phys. Fluids A* **1992**, *4*, 477–485.

(36) Diaz, M. E.; Fuentes, J.; Cerro, R. L.; Savage, M. D. *J. Colloid Interface Sci.* **2010**, *348*, 232–239.

(37) Padday, J. F.; Pitt, A. R. *Proc. R. Soc. London, Ser. A* **1972**, *329*, 421–431.

(38) Li, D.; Cheng, P.; Neumann, A. W. *Adv. Colloid Interface Sci.* **1992**, *39*, 347–382.

(39) Naydich, Yu. V.; Gab, I. I.; Evdokimov, V. A.; Kurkova, D. I.; Stetsyuk, T. V.; Grigorenko, N. F.; Chernigovtsev, E. P. *Powder Metall. Metal Ceram.* **2004**, *43*, 170–178.

(40) Dussan, E. B. *Ann. Rev. Fluid Mech.* **1979**, *11*, 371–400.

(41) Ehrhard, P.; Davis, S. H. *J. Fluid Mech.* **1991**, *229*, 365–388.

(42) Blokhuis, E. M. In *Surface and Interfacial Tension: Measurement, Theory, and Applications*; Hartland, S., Ed.; Surfactant Science Series 119; Marcel Dekker: New York, 2005; pp 147−193.

(43) Tadmor, R. *Surf. Sci.* **2008**, *602*, L108–L111.

(44) Bronshtein, I. N.; Semendyayev, K. A. *A Guide Book to Mathematics*; Springer-Verlag: New York, 1973.

(45) Picknett, R. G.; Bexon, R. J. *J. Colloid Interface Sci.* **1977**, *61*, 336–350.

(46) Erbil, H. Y.; Meric, R. A. *J. Phys. Chem. B* **1997**, *101*, 6867–6873.

(47) Gurtin, M. E. *Configurational Forces as Basic Concepts of Continuum Physics*; Applied Mathematical Sciences; Springer: New York, 2000; p 137.

(48) Maugin, G. A. *Appl. Mech. Rev.* **1995**, *48*, 213–245.

(49) Suo, Z. *Adv. Appl. Mech.* **1997**, *33*, 193–294.

(50) Berim, G. O.; Ruckenstein, E. *J. Phys. Chem. B* **2004**, *108*, 19330–19338.

(51) Bormashenko, E. *Colloids Surf., A* **2009**, *345*, 163–165.

(52) Boruvka, L.; Neumann, A. W. *J. Chem. Phys.* **1977**, *66*, 5464–5476.

(53) Blecua, P.; Lipowsky, R.; Kierfeld, J. *Langmuir* **2006**, *22*, 11041–11059.

(54) Widom, B. *J. Phys. Chem.* **1995**, *99*, 2803–2806.

(55) Glasner, K. B. *Phys. Fluids* **2003**, *15*, 1837–1842.

(56) Heine, D. R.; Grest, G. S.; Webb, E. B., III. *Phys. Rev. E* **2004**, *70*, 011606-1–10.

(57) Gomba, J. M.; Homsy, G. M. *Langmuir* **2009**, *25*, 5684–5691.